Scilight

Translational Insights
https://www.sciltp.com/journals/ti

Article

Mitochondrial Complex IV in Free form Controls Respiratory Channeling Independently of Supercomplex Assembly

Patrycja Anna Glogowski [1], Cristina Algieri [2,3], Antonia Cugliari [3], Maria Cotugno [4], Donatella Pietrangelo [5], Fabiana Trombetti [3], Micaela Fabbri [3], Speranza Rubattu [4,5] and Salvatore Nesci [3,*]

[1] Cardiovascular Medicine Unit, IRCCS Azienda Ospedaliero-Universitaria di Bologna, 40138 Bologna, Italy
[2] Department of Life Sciences, Health and Health Professions, Link University, 00165 Rome, Italy
[3] Department of Veterinary Medical Sciences, University of Bologna, 40064 Ozzano Emilia, Italy
[4] IRCCS Neuromed, 86077 Pozzilli, Italy
[5] Clinical and Molecular Department, Sapienza University of Rome, 00185 Roma, Italy
* Correspondence: salvatore.nesci@unibo.it

How To Cite: Glogowski, P.A.; Algieri, C.; Cugliari, A.; et al. Mitochondrial Complex IV in Free form Controls Respiratory Channeling Independently of Supercomplex Assembly. *Translational Insights* **2026**, *1*(1), 7.

Received: 27 March 2026
Revised: 19 April 2026
Accepted: 6 May 2026
Published: 12 May 2026

Abstract: Background: Mitochondrial respiratory efficiency is crucial for sustaining cellular energy production and oxidative balance. It depends not only on the assembly of electron transport chain complexes into supercomplexes, but also on the kinetic competence of their individual components. However, the functional significance of supercomplex assembly remains debated, particularly with regard to whether it ensures effective substrate channeling. Methods: In this study, we investigated the contribution of cytochrome *c* oxidase (Complex IV, CIV) to NADH-dependent respiratory flux in conditions where CIV is predominantly present in its free form rather than incorporated into the N-respirosome (CI+$CIII_2$+CIV) or the Q-respirosome ($CIII_2$+CIV). Metabolic flux analysis based on cyanide titration was used to assess the control exerted by CIV over the respiratory pathway. Results: Inhibition of CIV caused an exponential decline in both NADH-O_2 oxidoreductase and TMPD/ascorbate-O_2 oxidoreductase activities. The calculated flux control coefficient identified CIV as the rate-limiting step of NADH-supported respiration. Proteomic analysis further showed that, although both N-respirosomes and Q-respirosomes were present, CIV was predominantly detected in its free, non-assembled form, with only a minor proportion incorporated into supramolecular assemblies. These findings are consistent with the absence of effective kinetic substrate channeling between Complex I, Complex III, and CIV. Conclusions: These findings indicate that the functional state of CIV, rather than SC abundance alone, is a critical determinant of respiratory control and oxidative balance in mitochondria.

Keywords: mitochondrial respiratory supercomplexes; cytochrome *c* oxidase; substrate channeling; metabolic flux control analysis

1. Introduction

Mitochondrial oxidative phosphorylation depends on the coordinated activity of complexes I–IV and the mobile electron carriers coenzyme Q and cytochrome *c*, which together convert reducing equivalents into the proton-motive force that drives ATP synthesis [1]. Mitochondrial oxidative phosphorylation is central to cellular energy metabolism and redox homeostasis, sustaining ATP production while regulating key signaling and stress-

response pathways. Disruption of this process has been implicated in a wide spectrum of pathological conditions, including cardiovascular diseases, neurodegeneration, and cancer, highlighting the importance of understanding the determinants of respiratory efficiency. Despite major advances in the structural characterization of the electron transport chain, it remains unclear to what extent supramolecular organization into supercomplexes functionally optimizes electron transfer, as opposed to the intrinsic catalytic competence and distribution of individual respiratory complexes [2].

Beyond their individual catalytic properties, the respiratory complexes are organized in the inner mitochondrial membrane as higher-order assemblies, including the canonical respirasome (CI-$CIII_2$-CIV) and the $CIII_2$-CIV supercomplex [3–5]. Structural and biochemical studies have established that these arrangements are not static architectural curiosities, but regulated supramolecular states that can influence electron transfer, membrane organization, complex stability, and metabolic adaptation. At the same time, the functional meaning of supercomplex assembly remains debated, particularly with respect to whether supramolecular organization per se guarantees efficient substrate channeling between the redox partners of the chain [6].

This question is especially relevant for cytochrome *c* oxidase (complex IV, CIV), the terminal oxidase of the respiratory chain and the complex that couples electron transfer from reduced cytochrome *c* to oxygen reduction. Recent structural work has clarified how CIV is incorporated into mammalian $CIII_2$-CIV assemblies and how assembly factors such as SCAF1 contribute to the formation and conformational maturation of these supercomplexes [7,8]. Complementary mechanistic studies have refined the current model of electron transfer between CIII and CIV, indicating that supercomplexes can facilitate electron flux by constraining cytochrome *c* diffusion to a two-dimensional pathway on the supercomplex surface rather than by creating an obligatory sealed conduit [9]. Thus, supercomplexes may provide a kinetic advantage under some conditions, but they do not abolish the need to consider the abundance, exchange dynamics, and catalytic competence of the individual free complexes that coexist with the assembled states.

An additional level of complexity arises from the fact that respiratory supercomplex abundance is plastic and depends on tissue context, substrate availability, and metabolic state. In mammalian mitochondria, the relative partitioning of CIV between supercomplex-associated and free pools is therefore likely to have functional consequences that cannot be inferred from structure alone [5]. In particular, if CIV is present predominantly as a free complex rather than incorporated into the N-respirosome and Q-respirosome, the mere existence of supercomplexes may be insufficient to sustain effective kinetic channeling throughout the NADH-linked respiratory pathway. Under these conditions, flux control is predicted to shift toward the terminal oxidase segment, with free CIV becoming the bottleneck that limits overall NADH-O_2 respiration [10]. This framework is consistent with kinetic and flux-based analyses indicating that the respiratory chain can operate through partially distinct functional routes and that control of pathway flux depends on how mobile carriers and individual complexes are distributed between assembled and non-assembled states [10].

In this study, we address the role of CIV distribution in determining the efficiency of mitochondrial electron transfer. We test the hypothesis that, when CIV is not efficiently incorporated into the respirasome-type assemblies, supramolecular organization alone does not ensure effective channeling between complexes I, III, and IV. Instead, the free CIV pool becomes the rate-limiting step of the NADH-O_2 respiratory process, as revealed by metabolic flux analysis. By focusing on CIV not simply as the terminal catalyst of the chain but as a determinant of whether supercomplex organization is functionally productive, our work aims to refine current models of respiratory-chain compartmentation and to clarify the conditions under which supercomplexes enhance, rather than merely accompany, oxidative phosphorylation.

2. Material and Methods

2.1. Chemicals

Antimycin A, β-Nicotinamide adenine dinucleotide (NADH) and Sodium ascorbate (ASC) were obtained from Sigma–Aldrich (Milan, Italy). *N*,*N*,*N*′,*N*′-Tetramethyl-*p*-phenylenediamine dihydrochloride (TMPD) was purchased from Merck (Darmstadt, Germany). Quartz double distilled water was used for all reagent solutions.

2.2. Animal Model

A total of eight 10-week-old Wistar-Kyoto (WKY) rats were housed at the animal facility of La Sapienza University (Rome, Italy). The animals were fed a normal diet supplied by Lab. Piccioni (Milan, Italy), the composition of which has been described previously. Animals were subsequently euthanized according to a standardized protocol [11]. Hearts were collected immediately after sacrifice, snap-frozen in liquid nitrogen, and stored at −80 °C for molecular analyses. Animals were housed two to three per cage under controlled light,

temperature, and humidity conditions. All animal studies were performed in accordance with approved protocols by the IRCCS Neuromed Animal Care Review Board and the Istituto Superiore di Sanità (ISS permit number: 1086/2020) and were conducted according to EU Directive 2010/63/EU for animal experiments. The study is reported in accordance with the ARRIVE guidelines (https://arriveguidelines.org, accessed on 1 November 2024). WKY rats were selected because the present study was designed to investigate the basal organization of the mitochondrial respiratory chain and the contribution of free CIV to NADH-dependent flux control under non-pathological conditions. In this context, the use of a normotensive strain allowed us to examine the relationship between CIV distribution, supercomplex assembly, and respiratory channeling without the additional complexity introduced by hypertension-associated mitochondrial remodeling. Accordingly, a direct comparison with spontaneously hypertensive rats was beyond the scope of this work, which was conceived as a mechanistic study focused on basal mitochondrial function in heart.

2.3. Preparation of Rat Heart Mitochondria

Heart rat mitochondria were isolated as described by Algieri et al. [12]; the protocol was adapted to rat species with some modifications. Briefly, a pool of three to four thawed rat hearts was initially weighed and gently dried on blotting paper. Then finely chopped into small pieces with scissors and homogenized by Ultraturrax T25 in ice-cold Tris-HCl buffer (medium B) consisting of 0.25 M sucrose, 10 mM Tris, 1 mM EDTA (free acid), 0.5 mg/mL BSA fatty acid free, pH 7.4 with HCl at a ratio of 10 mL medium B per 1 g of tissue. The homogenate was centrifuged to remove nuclei and plasma membrane fragments (Sorvall RC2-B, rotor SS34) at 3000 rpm for 5 min at 4 °C. The pellet was re-homogenized and centrifuged at the same conditions, and the whole supernatant obtained first was filtered via four cotton gauze layer and then centrifuged at 10,000 rpm for 10 min at 4 °C. The pellet was resuspended with medium A consisting of 0.25 M sucrose, 10 mM Tris(hydroxymethyl)-aminomethane (Tris), pH 7.4 with HCl and re-centrifuged under the same conditions. Finally, the pellet was resuspended by gentle stirring using a Teflon Potter Elvejehm homogenizer in a small volume of medium A. All steps were carried out at 0–4 °C. The mitochondrial protein determination was performed with the colorimetric method described by Bradford by Bio-Rad Protein Assay kit II with bovine serum albumin BSA as standard [13]. Then, the mitochondrial aliquots were stored in liquid nitrogen.

2.4. Metabolic Flux Control Analysis

Determinations of flux control coefficients and threshold plots were studied by titrating the whole respiratory chain activity performing NADH-O_2 oxidoreductase activity and single steps with inhibitor KCN for CIV performing TMPD/ASC-O_2 oxidoreductase activity [10]. To detect mitochondrial respiratory activities, the oxygen consumption rates were polarographically evaluated by Clark-type electrode using a thermostated Oxytherm System (Hansatech Instruments, King's Lynn, UK) equipped with a 1 mL polarographic chamber. The reaction mixture (120 mM KCl, 10 mM Tris-HCl buffer pH 7.2), maintained under Peltier at a fixed temperature (37 °C) and continuous stirring, contained 0.25 mg mitochondrial protein. Evaluation of NADH-O_2 oxidoreductase activity was performed in presence of different concentrations of KCN using the 75 µM NADH substrate. Similarly, TMPD/ASC-O_2 oxidoreductase activity by CIV was evaluated in presence of 0.5 mM TMPD + 2 mM ASC by detecting the cytochorme *c* oxidation in the presence of 1 µg/mL antimycin A. KCN concentrations for the titration curves range from 0 to 2 mM, depending on the reactivity of the sample group threshold plots were derived from titration curves by plotting the relative rate of the global respiratory activity (NADH-O_2 oxidoreductase) as a function of the percentage inhibition of the single-step activity of complex IV (TMPD/ascorbate-O_2 oxidoreductase), determined at identical inhibitor concentrations [10]. Control coefficients (C_i) were calculated as the ratio between the slope of the inhibition curve of the global flux (J) and the slope of the inhibition curve of the complex IV (CIV) [10].

$$C_i = \frac{(\mathrm{d}\,J/\mathrm{d}\,I)_{I=0}}{(\mathrm{d}\,v_i/\mathrm{d}\,I)_{I=0}}$$

2.5. Proteomic Analysis

Bidimensional proteomic analysis was performed using the isolated mitochondrial fraction stored in liquid nitrogen, as described by Cugliari, Algieri, Glogowski et al.[14]. Frozen aliquots were thawed and centrifuged using a TJ-25 Beckman Coulter centrifuge (rotor A-15) at 11,000×*g* for 15 min at 4 °C. The resulting pellet was resuspended in resuspension buffer (50 mM NaCl, 50 mM imidazole, 5 mM 6-aminohexanoic acid, pH 7.0) to obtain a final protein concentration of 3.35 mg/mL. For the detergent titration, 10 µg of protein was incubated with

increasing amounts of digitonin at detergent-to-protein ratios of 10, 8, 6, and 4 g/g. Optimal solubilization was achieved at a ratio of 4 g/g. Samples were incubated on ice for 20 min and subsequently centrifuged at 20,000×*g* for 20 min at 4 °C. An aliquot of 5 µL of the supernatant was used to determine protein concentration by the Bradford assay [13]. The remaining supernatant was supplemented with 11% glycerol, 5% Coomassie G-250 (with a Coomassie-to-detergent ratio of 1:10, mg/mg), and water, and then loaded into the wells of precast 10-well NativePAGE 3–12% Bis-Tris mini gels (1.0 mm thickness; Thermo Fisher Scientific, Waltham, MA, USA). 7 µL of NativeMark Unstained Protein Standard (Thermofisher Scientific, Waltham, MA, USA) was loaded per gel. First-dimension electrophoresis was performed under native conditions using a 3–12% gradient blue native gel. Briefly, the first third of the BN-PAGE run was performed at a constant 70 V using a dark blue cathode buffer, after which the buffer was switched to light blue cathode buffer and the gel run at 150 V until completion. Thus, the gel was washed with MilliQ water, and read at the ChemiDoc. A selected gel strip from unfixed gel was subjected to sequential chemical treatments to achieve denaturing conditions. First, the strip was incubated for 30 min at 37 °C in a reducing buffer containing 4× NuPAGE LDS buffer, MilliQ water, and 50 mM 2-mercaptoethanol under a chemicalhood. This buffer was replaced with an alkylation buffer (4× NuPAGE LDS Buffer, 54.32 mM *N*,*N*-dimethylacrylamiden and MilliQ water) for 30 min and then with a quenching buffer (4× NuPAGE LDS Buffer, NuPAGE sample reducing agent 10×, 19.2% ethanol and MilliQ water) for 30 min. Then, the gel was washed with MilliQ water prior to being set on top of a NuPAGE 4–12%, Bis-Tris, 1.0–1.5 mm, Mini Protein Gels. Exactly 5 µL of Biotinylated Protein Ladder (81851, Cell Signalling Technology, Danvers, MA, USA) was placed in the control well. The SDS-PAGE gel was run at 100 V constant for 15 min, then 150 V constant until the end of the run. The gel was incubated for 30 min with 1× Tris-glycine to be transferred to a 0.2 µm nitrocellulose membrane (Trans-Blot Turbo Mini 0.2 µm Nitrocellulose Transfer Packs, BioRAD, Hercules, CA, USA) using the mixed molecular weight 1.3°-25V-7′ protocol of a Trans-Blot Turbo Transfer System (BioRAD). The mem-brane was blocked for 1 h with 5% milk in 1× PBS added with 0.1% Tween 20. Complex I, Complex III, and CIV were detected using the following primary antibodies: for CI, 1:1000 diluted mouse anti-NDUFA9 mono-clonal antibody (clone: 20C11B11B11, 459100, Thermofisher, Waltham, MA, USA); for CIII, 1:1000 diluted mouse anti-UQCRFS1 monoclonal antibody (clone: OTI4H8, MA5-27471, Thermofisher); for CIV, 1:1000 diluted mouse anti-MTCO1 monoclonal antibody (clone: E7A11, bsm-60242M, CliniSciences, Nanterre, France). All the antibodies were diluted in TBS-Tween20, consisting of 150 mM NaCl, 50 mM Tris–HCl, and 1% Tween20, and were incubated overnight at 4 °C. Following incubation with goat anti-mouse IgG (H + L) cross-adsorbed secondary antibody diluted 1:10,000 (G-21040, Thermofisher) together with anti-biotin, HRP-linked antibody (7075, Cell Signalling Technology) diluted 1:1000, visualization at the ChemiDoc was performed following 5 min incubation with ECL (Clarity Western ECL substrate, BioRad). The spots of the 2D gel obtained after Western blotting analysis on subunits of respiratory complexes have been detected and quantified by using ImageLab software 6.1 [10].

2.6. Statistical Analysis

Data are presented as mean ± standard deviation (SD) for three experimental group each consisting of trhee animals. Statistical comparisons among groups were carried out using one-way analysis of variance (ANOVA), followed by Bonferroni's post hoc test. A p value < 0.05 was considered statistically significant.

3. Results

To define the distribution of metabolic control along the NADH-dependent respiratory pathway, flux control analysis was performed by comparing the inhibitory effects of KCN on NADH-O_2 oxidoreductase activity and on TMPD/ascorbate-O_2 oxidoreductase activity.

As shown in Figure 1A, KCN titration of NADH-O_2 oxidoreductase activity produced a progressive decrease in activity that followed an exponential inhibition profile. A similar exponentially decreasing trend was observed for TMPD/ascorbate-O_2 oxidoreductase activity in Figure 1B. The slopes derived from the nonlinear fits of the two titration curves were used to estimate the flux control coefficient of CIV on the overall NADH-supported respiratory flux. The resulting *Ci* value of 0.17 indicates that CIV exerts the predominant control over the NADH-O_2 oxidoreductase pathway. This behavior is consistent with the lack of effective substrate channeling between Complex I and CIV, implying that reducing equivalents generated from NADH are not efficiently transferred through a kinetically insulated supramolecular route to oxygen. Instead, CIV behaves as the rate-limiting step of the entire electron-transfer sequence.

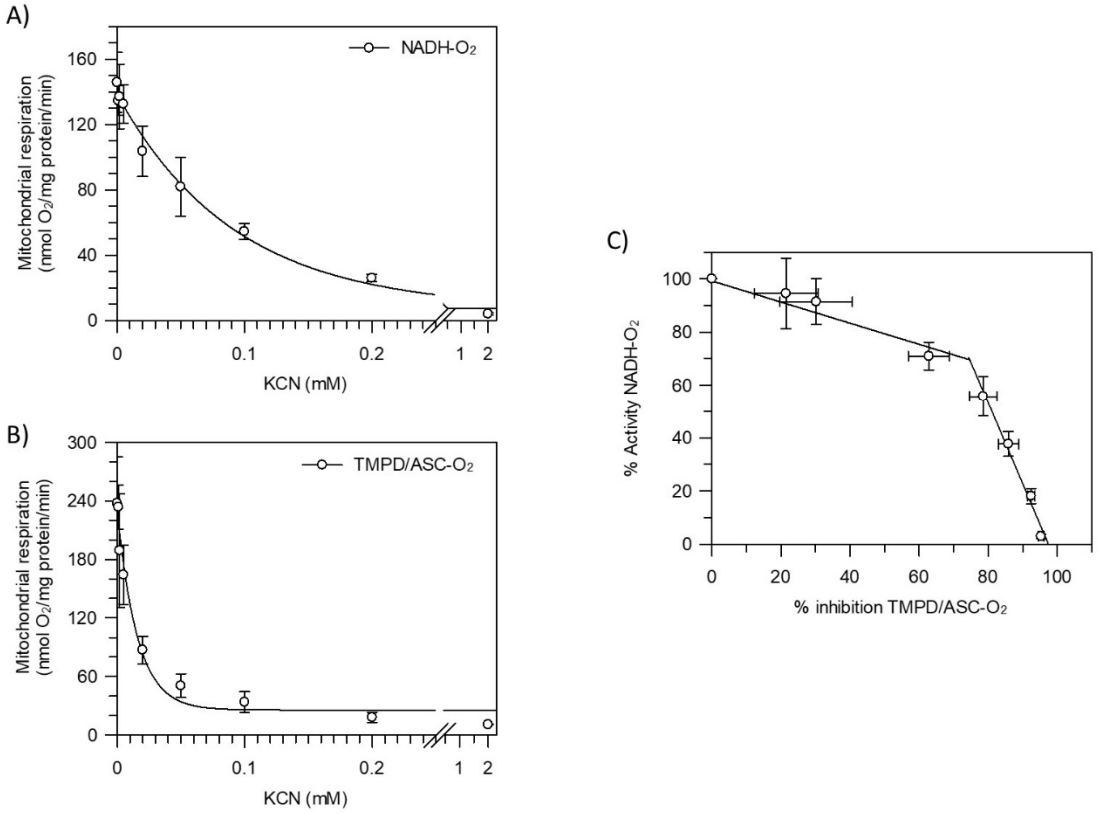

Figure 1. KCN titration reveals flux control of NADH-supported respiration by CIV. (**A**) Inhibition of NADH-O_2 oxidoreductase activity by increasing KCN concentration. (**B**) Inhibition of TMPD/ascorbate-O_2 oxidoreductase activity by KCN. (**C**) Threshold plots of NADH oxidase activity where each point represents the % activity of aerobic NADH oxidation with Complex I as a function of % inhibition TMPD/ASC-O_2 with CIV for the same KCN concentration. The respiratory substrates sustaining the mitochondrial respiration were 75 μM NADH for Complex I and 0.5 mM TMPD/2 mM ASC. All points represent the mean ± SD (vertical bars in **A** and **B**) and (vertical and horizontal bars in **C**) from three independent experiments carried out on different mitochondrial preparations obtained from groups of three animals.

This conclusion was further supported by threshold analysis. In Figure 1C, the percentage of residual NADH-O_2 oxidoreductase activity was plotted against the percentage inhibition of TMPD/ascorbate-O_2 oxidoreductase activity measured at the same KCN concentrations. The resulting relationship was piecewise linear and showed no evident threshold region or deviation from proportionality. Thus, inhibition of CIV was directly mirrored by inhibition of the overall NADH-driven respiratory flux. This proportional response confirms that no detectable channeling operates along the NADH oxidation pathway under these conditions. Taken together, these data demonstrate that the limited catalytic capacity of CIV constrains the maximal flux through the entire Complex I-to-CIV sequence, identifying CIV as the main site of control of NADH-dependent respiration.

To further investigate the supramolecular organization of the respiratory chain, despite the functional evidence against substrate channeling obtained in Figure 1, we conducted a comprehensive proteomic analysis of mitochondrial supercomplexes. This analysis aimed to quantify the distribution of the respiratory complexes between their free forms and their supramolecular assemblies, thereby assessing whether the structural arrangement of the complexes might theoretically enable channeling, even if functionally undetected. Figure 2A displays the proteomic identification of the major supercomplexes, revealing the presence of both N-respirosomes (composed of CI-$CIII_2$-CIV) and Q-respirosomes (containing $CIII_2$-CIV). These supramolecular assemblies confirm that mitochondria organize part of their respiratory machinery into higher-order structures. However, the detection of these architectures contradicts the findings from Figure 1, which demonstrated the absence of NADH-to-O_2 channeling based on a low flux control coefficient (Ci = 0.17). Instead, the structural data complement the functional assays by showing that the mere presence of supercomplexes is not sufficient to guarantee an effective channeling pathway.

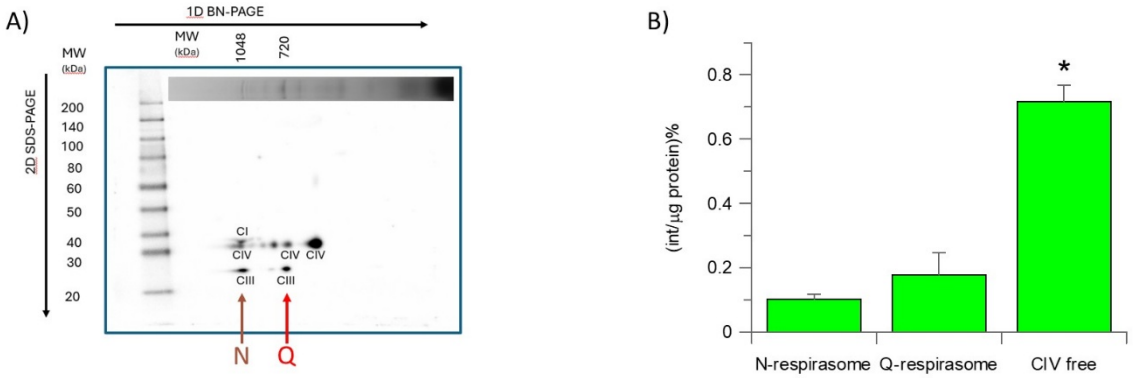

Figure 2. Supramolecular organization of respiratory complexes in heart mitochondria rat detected by 2D BN/SDS-PAGE. In (**A**) the arrows on 2D SDS-PAGEs show the position of N-respirasome (N) (CI-$CIII_2$-CIV) and Q-respirasome (Q) ($CIII_2$-CIV). The antibodies are against NDUFA9 (36 kDa) subunit of Complex I, UQCRFS1 (25 kDa) subunit of Complex III, and MTCO1 (35 kDa) subunit of CIV. (**B**) Quantification and ratio of in N and Q superassembly and in CIV free form not involved in supercomplexes. Vertical bars represent the mean ± SD from three independent experiments carried out on different mitochondrial preparations obtained from groups of three animals. * indicate significantly different ($p < 0.05$).

The quantitative analysis presented in Figure 2B provides a key mechanistic interpretation. When comparing the abundance of respiratory complexes incorporated into the N- and Q-respirosomes with the total amount of each complex, we observe that the fraction of complexes engaged in supramolecular assemblies is significantly smaller than the pool of free CIV. Notably, CIV is predominantly found in its free, non-assembled form, with only a minor proportion incorporated into N- and/or Q-respirosome. This imbalance indicates that the overall stoichiometry of the respiratory chain strongly favors free CIV over assembled supercomplexes. This finding offers a plausible explanation for the kinetic limitation observed in Figure 1. The modest incorporation of CIV into supramolecular structures suggests that CIV remains rate-limiting because only a small fraction of it participates in supercomplexes, while the majority acts independently. Consequently, any potential channeling effect that would depend on a stable and abundant respirosome architecture is effectively masked by the limited quantitative contribution of these structures. Thus, the proteomic evidence from Figure 2 supports and refines the functional interpretation: although N- and Q-respirosomes are present, they exist in quantities too small to generate a physiologically relevant substrate-channeling mechanism under the experimental conditions tested. These data identify the low stoichiometric incorporation of CIV into N- and Q-respirosomes as the key factor limiting the functional impact of supercomplexes, thereby explaining why their structural presence does not result in physiologically relevant substrate channeling.

4. Discussion

The present data indicate that the supramolecular organization of the respiratory chain is not, by itself, sufficient to ensure functional substrate channeling along the NADH-dependent pathway. Functionally, the low flux control coefficient obtained from KCN titration ($Ci = 0.17$) and the absence of a threshold in the inhibition plot show that inhibition of CIV is transferred almost proportionally to the overall NADH-O_2 flux. In metabolic-control terms, this means that CIV retains dominant control over the pathway and behaves as the rate-limiting step of electron transfer from NADH to oxygen, rather than serving as the terminal acceptor of a kinetically protected CI-to-CIV channel. This interpretation is consistent with previous flux analyses showing that the NADH-fed pathways can remain at least partially segregated and that the control exerted by CIV depends on how the mobile carriers and respiratory complexes are distributed between free and supercomplex-associated pools [10,15].

These functional results are particularly informative when considered together with the proteomic evidence. Figure 2 shows that N-respirosomes and Q-respirosomes are present, but also that most CIV is not incorporated into those assemblies and instead remains in the free pool. This quantitative imbalance provides the mechanistic explanation for the lack of detectable channeling. Structural studies have established that mammalian mitochondria can form CI-$CIII_2$-CIV respirasomes and $CIII_2$-CIV assemblies, and that SCAF1 contributes to the formation of $CIII_2$-CIV supercomplexes; however, the functional meaning of these assemblies depends on their abundance, stability, and exchange kinetics, not merely on their existence [1,3,5,16]. In this context, the predominance of free CIV implies that only a minor fraction of the respiratory chain is organized into a configuration potentially compatible with facilitated cytochrome *c* transfer, whereas the bulk of electron flux must traverse a pathway in

which diffusion through the general cytochrome *c* pool remains obligatory and CIV availability becomes limiting. This conclusion also fits the current view that supercomplexes do not create an obligatorily sealed conduit for electrons. Rather, they may facilitate electron transfer under some conditions by constraining cytochrome *c* diffusion to a two-dimensional route along the supercomplex surface. In yeast, cryo-EM and kinetic analysis support such a 2D diffusion mechanism between CIII and CIV, showing that the kinetic advantage derives from local confinement of cytochrome *c* rather than from complete isolation from the bulk phase [9,17]. Therefore, when CIV is only weakly represented within N- and Q-respirosomes, any local advantage conferred by supercomplex architecture is expected to be diluted at the level of the total respiratory flux. Under these circumstances, the pathway behaves kinetically as a largely non-channeled system, despite the structural presence of supercomplexes. This point is in line with broader analyses arguing that the existence of supercomplexes should not automatically be equated with effective substrate channeling [6].

An important consequence of this organization is impaired respiratory efficiency. When electrons derived from NADH cannot be transferred through a sufficiently abundant and kinetically favored CI-$CIII_2$-CIV route, the overall flux becomes more vulnerable to diffusional constraints and to mismatches between upstream electron supply and downstream oxidase capacity. In practical terms, Complex I and Complex III can become relatively more reduced because the terminal oxidase step cannot clear electrons fast enough. This favors accumulation of reduced intermediates upstream of CIV, lowering the efficiency with which NADH oxidation support oxygen consumption. Experimental and conceptual studies of respiratory supercomplexes have repeatedly linked proper supramolecular organization with improved respiratory efficiency and with more effective coordination among chain segments [18].

The redox consequences of this bottleneck are also relevant for ROS production. Mitochondrial ROS generation increases when electron carriers upstream of oxygen are highly reduced and when electron transfer is slowed, because electron leak to oxygen becomes more probable at major ROS-producing sites, especially Complex I and Complex III [19,20]. In the scenario emerging from our data, the absence of effective channeling does not simply reduce flux; it is expected to increase the residence time of electrons within upstream redox centers. A CIV bottleneck would therefore favor over-reduction of the NADH/NAD^+ and coenzyme Q pools and promote electron leak, particularly when demand for ATP is limited or when membrane potential remains high. Under these conditions, the loss of kinetically efficient electron transfer can be directly coupled to increased ROS formation [21].

This interpretation is consistent with the idea that respiratory supercomplex organization may help minimize ROS not because supercomplexes are universally mandatory for catalysis, but because they can decrease electron leak by improving the matching between electron input and output. In fact, the proposal that supercomplex association limits ROS production from Complex I has been explicitly advanced [22]. ROS protection should not be attributed to supercomplex presence in a binary manner; rather, it depends on whether enough CIV is actually engaged in the relevant supramolecular assemblies to support kinetically meaningful electron transfer. If most CIV remains free, the chain may retain structural supercomplexes yet still operate functionally as a poorly channeled system, with impaired flux and increased propensity for ROS generation. More broadly, these findings support a model in which CIV distribution is a decisive variable in respiratory-chain compartmentation. In this model, the balance between free and supercomplex-associated CIV determines whether the chain behaves as an integrated high-flux NADH oxidation pathway or as a system in which terminal oxidase capacity imposes a bottleneck on upstream redox segments. This view is compatible with the recognized plasticity of respiratory supercomplexes and with the notion that their physiological role is context-dependent rather than universal [1,6,23]. Accordingly, the results might argue that free CIV is not just a passive excess pool but a key determinant of respiratory performance. When it predominates over assembled CIV, the respiratory chain loses effective channeling, NADH-supported flux becomes constrained by the terminal oxidase step, and the conditions favoring mitochondrial ROS production are enhanced.

On balance, the present findings should be interpreted in light of some inherent limitations of the experimental approach. The combination of flux-control analysis, inhibitor titration, and proteomic profiling provides a coherent functional and structural framework to assess the role of CIV in NADH-dependent respiration under the conditions examined here. Within this framework, the absence of effective substrate channeling is supported by a consistent indirect signature rather than by a direct measurement of electron-transfer routes, and the relative functional contribution of free versus supercomplex-associated CIV cannot be resolved directly. Likewise, although KCN titration is informative with respect to pathway control, it does not by itself fully define the underlying mechanism. The implications for oxidative balance and ROS generation are therefore discussed as plausible consequences of the respiratory organization [24].

Beyond its mechanistic implications, this organization may be particularly relevant in the cardiovascular setting, where mitochondrial function is tightly coupled to myocardial energetic homeostasis. In human heart failure, mitochondrial dysfunction is increasingly recognized as a central contributor to disease progression rather than a secondary consequence of impaired contractile performance. In this context, when the terminal oxidase step cannot clear electrons fast enough, Complex I and Complex III can become relatively more reduced, thereby favoring electron leak and ROS generation [25]. The distribution of CIV between free and supercomplex-associated states may therefore represent a functionally relevant determinant of mitochondrial performance in the myocardium [26].

Author Contributions

P.A.G.: investigation, methodology, writing—original draft; C.A.: validation, writing—reviewing and editing; A.C.: data curation, writing—reviewing and editing; M.C.: methodology; D.P.: methodology; F.T.: writing—reviewing and editing; M.F.: investigation; S.R.: conceptualization, visualization; S.N.: conceptualization, supervision; validation, writing—original draft. All authors have read and agreed to the published version of the manuscript.

Institutional Review Board Statement

All animal studies were performed in accordance with approved protocols by the IRCCS Neuromed Animal Care Review Board and the Istituto Superiore di Sanità (ISS permit number: 1086/2020) and were conducted according to EU Directive 2010/63/EU for animal experiments.

Informed Consent Statement

Not applicable.

Data Availability Statement

The datasets generated and analyzed during the current study are available from the corresponding author on reasonable request.

Conflicts of Interest

The authors declare no conflict of interest.

Use of AI and AI-Assisted Technologies

No AI tools were utilized for this paper.

References

1. Vercellino, I.; Sazanov, L.A. The assembly, regulation and function of the mitochondrial respiratory chain. *Nat. Rev. Mol. Cell Biol.* **2022**, *23*, 141–161. https://doi.org/10.1038/s41580-021-00415-0.
2. Suomalainen, A.; Nunnari, J. Mitochondria at the crossroads of health and disease. *Cell* **2024**, *187*, 2601–2627. https://doi.org/10.1016/j.cell.2024.04.037.
3. Gu, J.; Wu, M.; Guo, R.; et al. The architecture of the mammalian respirasome. *Nature* **2016**, *537*, 639–643. https://doi.org/10.1038/nature19359.
4. Wu, M.; Gu, J.; Guo, R.; et al. Structure of Mammalian Respiratory Supercomplex $I_1III_2IV_1$. *Cell* **2016**, *167*, 1598–1609.e10. https://doi.org/10.1016/j.cell.2016.11.012.
5. Vercellino, I.; Sazanov, L.A. Structure and assembly of the mammalian mitochondrial supercomplex $CIII_2CIV$. *Nature* **2021**, *598*, 364–367. https://doi.org/10.1038/s41586-021-03927-z.
6. Milenkovic, D.; Blaza, J.N.; Larsson, N.-G.; et al. The Enigma of the Respiratory Chain Supercomplex. *Cell Metab.* **2017**, *25*, 765–776. https://doi.org/10.1016/j.cmet.2017.03.009.
7. Vercellino, I.; Sazanov, L.A. SCAF1 drives the compositional diversity of mammalian respirasomes. *Nat. Struct. Mol. Biol.* **2024**, *31*, 1061–1071. https://doi.org/10.1038/s41594-024-01255-0.
8. García-Poyatos, C.; Cogliati, S.; Calvo, E.; et al. Scaf1 promotes respiratory supercomplexes and metabolic efficiency in zebrafish. *EMBO Rep.* **2020**, *21*, e50287. https://doi.org/10.15252/embr.202050287.

9. Moe, A.; Di Trani, J.; Rubinstein, J.L.; et al. Cryo-EM structure and kinetics reveal electron transfer by 2D diffusion of cytochrome *c* in the yeast III-IV respiratory supercomplex. *Proc. Natl. Acad. Sci. USA* **2021**, *118*, e2021157118. https://doi.org/10.1073/pnas.2021157118.
10. Nesci, S.; Algieri, C.; Trombetti, F.; et al. Two separate pathways underlie NADH and succinate oxidation in swine heart mitochondria: Kinetic evidence on the mobile electron carriers. *Biochim. Biophys. Acta Bioenerg.* **2023**, *1864*, 148977. https://doi.org/10.1016/j.bbabio.2023.148977.
11. Rubattu, S.; Di Castro, S.; Schulz, H.; et al. Ndufc2 Gene Inhibition Is Associated With Mitochondrial Dysfunction and Increased Stroke Susceptibility in an Animal Model of Complex Human Disease. *J. Am. Heart Assoc.* **2016**, *5*, e002701. https://doi.org/10.1161/JAHA.115.002701.
12. Algieri, C.; Cugliari, A.; Granata, S.; et al. Dextromethorphan Is a Novel Pharmacological Inhibitor of F_1FO-ATPase That Targets the Membrane-Embedded Domain Impairing ATP Synthesis and Hydrolysis. *Biofactors* **2026**, *52*, e70076. https://doi.org/10.1002/biof.70076.
13. Bradford, M.M. A rapid and sensitive method for the quantitation of microgram quantities of protein utilizing the principle of protein-dye binding. *Anal. Biochem.* **1976**, *72*, 248–254. https://doi.org/10.1016/0003-2697(76)90527-3.
14. Cugliari, A.; Algieri, C.; Glogowski, P.A.; et al. The Function and Supramolecular Assembly of the Mitochondrial Respiratory Complexes Underlie Hypertension-Related Stroke Susceptibility in a Model of Complex Human Disease. *Biofactors* **2025**, *51*, e70055. https://doi.org/10.1002/biof.70055.
15. Bianchi, C.; Genova, M.L.; Parenti Castelli, G.; et al. The mitochondrial respiratory chain is partially organized in a supercomplex assembly: Kinetic evidence using flux control analysis. *J. Biol. Chem.* **2004**, *279*, 36562–36569. https://doi.org/10.1074/jbc.M405135200.
16. Genova, M.L.; Lenaz, G. Functional role of mitochondrial respiratory supercomplexes. *Biochim. Biophys. Acta* **2014**, *1837*, 427–443. https://doi.org/10.1016/j.bbabio.2013.11.002.
17. Brzezinski, P.; Moe, A.; Ädelroth, P. Structure and Mechanism of Respiratory III-IV Supercomplexes in Bioenergetic Membranes. *Chem. Rev.* **2021**, *121*, 9644–9673. https://doi.org/10.1021/acs.chemrev.1c00140.
18. Cogliati, S.; Frezza, C.; Soriano, M.E.; et al. Mitochondrial cristae shape determines respiratory chain supercomplexes assembly and respiratory efficiency. *Cell* **2013**, *155*, 160–171. https://doi.org/10.1016/j.cell.2013.08.032.
19. Hernansanz-Agustín, P.; Enríquez, J.A. Generation of Reactive Oxygen Species by Mitochondria. *Antioxidants* **2021**, *10*, 415. https://doi.org/10.3390/antiox10030415.
20. Genova, M.L.; Lenaz, G. The Interplay Between Respiratory Supercomplexes and ROS in Aging. *Antioxid. Redox Signal.* **2015**, *23*, 208–238. https://doi.org/10.1089/ars.2014.6214.
21. Murphy, M.P. How mitochondria produce reactive oxygen species. *Biochem. J.* **2009**, *417*, 1–13. https://doi.org/10.1042/BJ20081386.
22. Maranzana, E.; Barbero, G.; Falasca, A.I.; et al. Mitochondrial respiratory supercomplex association limits production of reactive oxygen species from complex I. *Antioxid. Redox Signal.* **2013**, *19*, 1469–1480. https://doi.org/10.1089/ars.2012.4845.
23. Lenaz, G.; Nesci, S.; Genova, M.L. Understanding differential aspects of microdiffusion (channeling) in the Coenzyme Q and Cytochrome *c* regions of the mitochondrial respiratory system. *Mitochondrion* **2024**, *74*, 101822. https://doi.org/10.1016/j.mito.2023.11.005.
24. Cogliati, S.; Cabrera-Alarcón, J.L.; Enríquez, J.A. Regulation and functional role of the electron transport chain supercomplexes. *Biochem. Soc. Trans.* **2021**, *49*, 2655–2668. https://doi.org/10.1042/BST20210460.
25. Ramírez-Camacho, I.; Correa, F.; El Hafidi, M.; et al. Cardioprotective strategies preserve the stability of respiratory chain supercomplexes and reduce oxidative stress in reperfused ischemic hearts. *Free Radic. Biol. Med.* **2018**, *129*, 407–417. https://doi.org/10.1016/j.freeradbiomed.2018.09.047.
26. Hinton, A.; Claypool, S.M.; Neikirk, K.; et al. Mitochondrial Structure and Function in Human Heart Failure. *Circ. Res.* **2024**, *135*, 372–396. https://doi.org/10.1161/CIRCRESAHA.124.323800.